Journal of Sound and Vibration 329 (2010) 4422–4439

Contents lists available at ScienceDirect

Journal of Sound and Vibration

journal homepage: www.elsevier.com/locate/jsvi

Dynamic and acoustic response of bidirectionally stiffened plates with eccentric stiffeners subject to airborne and structure-borne excitations

Abderrazak Mejdi *, Noureddine Atalla

GAUS, Department of Mechanical Engineering, University de Sherbrooke, Sherbrooke, Que., Canada J1K 2R1

ARTICLE INFO

Article history:
Received 28 April 2009
Received in revised form
5 April 2010
Accepted 7 April 2010
Handling Editor: M.P. Cartmell
Available online 8 June 2010

ABSTRACT

An analytical method based on the modal expansion technique was developed to predict the vibro-acoustic response of both unidirectionally and bidirectionally stiffened flat panel. This paper presents the response to diffuse acoustic field (DAF) and turbulent boundary layer (TBL) excitations in terms of their joint acceptance. Numerical results for the dynamic and acoustic responses are compared with finite element method (FEM) and boundary element (BEM) results for stiffened panel with complex and eccentrically shaped stiffeners subject to point force excitation. A theoretical prediction of the transmission loss (TL) is also compared with laboratory measurements conducted on flat panels representing aircraft models as well as with hybrid statistical energy analysis (SEA)–FEM periodic model. The results confirm that the stiffened panel has the same acoustic response as the skin without stiffeners at frequencies where the structural wavelengths are equal to the spacing between the stiffeners. In addition, the transmission loss is lowered by the presence of the stiffeners at some particular region of frequencies below the critical frequency with respect to the unstiffened panel.

1. Introduction

Unlike the vibro-acoustic response of simple continuous structures such as beams and plates [1,2], a detailed analysis of wave motions for stiffened plates is often difficult to achieve because of the complexity of the structural configuration and the uncertainty of the boundary conditions. Traditionally, the vibration of a periodic plate structure is analyzed using an equivalent orthotropic plate [1,3]. Heckl [4] has suggested that a periodic ribbed plate could be treated as an orthotropic plate when the distance between the adjacent ribs is less than a quarter of the shortest plate-bending wavelength. Based on the calculation of wave propagating constants, he found that pass bands of a periodic ribbed plate could be divided into two categories: the first one is close to the resonance frequencies of the un-ribbed plate, while the second is close to the frequencies of total transmission for a plate with one beam. The orthotropic model is therefore more appropriate at lower frequencies. The most common approaches to analyzing the dynamic response of periodic structures are wave propagation [4–6], transfer matrix method [7,8], spectral finite elements [14], finite element method (FEM) [9–12] and boundary element method (BEM) [13]. The two latter methods are deterministic, thus providing accurate numerical tools for predicting the dynamic response of ribbed plates with complex configurations.

* Corresponding author. Tel.: +1 819 821 8000x62673.
E-mail address: abderrazak.mejdi@usherbrooke.ca (A. Mejdi).

0022-460X/$ - see front matter Crown Copyright © 2010 Published by Elsevier Ltd. All rights reserved.
doi:10.1016/j.jsv.2010.04.007

To predict the vibro-acoustics of ribbed panels in the context of statistical energy analysis (SEA), Bremner [22] has explained the distinct behaviors in terms of wavenumbers of a flat ribbed plate of width L_x and height L_y stiffened with ribs and frames with spacing S_y and S_x between the ribs and frames. As the modal half-wavelength in the x and y-direction goes below the L_x and L_y dimensions, the plate behavior shifts from global behavior, over the plate area (L_x, L_y), to periodic behavior over areas delimited by (L_x, S_y), (L_y, S_x). Finally, when the modal half-wavelength goes below the rib and frame spacing S_x and S_y, the modal behavior is determined by the behavior of a flat uniform sub-panel delimited by the ribs and frames. Those four conditions represent the four models required in fully describing the modal behavior of a stiffened plate over a large frequency band. When a particular condition is met for periodic modes behavior, modes will exist in groups of multiplicity μ_p. The multiplicity factor is the number of modes that are sustained at a particular frequency. Recently, Cotoni et al. [23] developed a hybrid (SEA) subsystem formulation based on finite elements, component mode synthesis and periodic theory to evaluate modal density and coupling loss factor of ribbed plates. The analytical model presented in this paper will be compared to previous model.

Maidanik [24] evaluated the response of a ribbed plate excited by a diffuse field. He found that ribbing increases the radiation resistance of the panel and therefore enhances the energy exchange between the panel and the sound field. Fahy [25] concurs by stating that the wave reflections produced by the ribs alter the dispersion relationship in such a way that free waves having wavenumber vector components of supersonic phase velocity can propagate at frequencies below the critical frequency of the uniform-plate. These components increase the subcritical radiation efficiency and may cause the panel to be excited in a coincident manner by incident sound waves at frequencies below coincidence, thus decreasing transmission loss.

Several analytical models have been developed. Lee and Kim [15] modeled the stiffeners using a combination of lumped masses and translational and rotational springs to evaluate the sound transmission loss by means of the spatial harmonic technique developed by Mead and Pujara [16] and Mead [17,18]. This model does not take into account the geometry of the stiffeners. In addition, their numerical results were not validated experimentally. Maurys and Matte [19] added the stiffeners onto the plate as a force, but they did not take the moment into account. Lin and Pan [20] and Lin [21] modeled the stiffeners of simply supported plates as forces and moments and investigated the forced vibration properties of unidirectionally stiffened flat plates at low frequency range. Liu et al. [36] used the receptance method and modal expansion technique to evaluate the airborne sound insulation of curved panels with a stringer and frame attachments. The acoustic diffuse field response of the stiffened panels was analyzed. The formulation for the bidirectionally stiffened panels was given in the same way as for the unidirectionally stiffened panels. In their analysis, the effect of circumferential stiffeners was neglected and the bidirectionally stiffened panels were treated as the unidirectional stiffened one.

In this paper, a semi-analytical formulation based on the modal expansion technique is presented to predict the vibro-acoustic response of both unidirectionally and bidirectionally stiffened flat plates with even and uneven inter-rib spacing. The formulation is an extension of previous modal-based works accounting for the interactions between ribs and plate as moments and force coupling. The rotary inertia of the skin is taken into account and the method to accommodate the eccentricity of the stiffeners about the mid-plane is clearly defined. Moreover, the effect of the cross-modal coupling on the vibro-acoustic response of stiffened plate is investigated. The interaction between the orthogonal stiffeners in the case of the bidirectionally stiffened plate is clearly captured in the presented formulation. The presented method allows a reliable estimate of the responses to different types of excitations such as point force, DAF and TBL. It is worth noting here that while there is an extensive literature on the response of isotropic flat plates to TBL excitation [26,27], only a few published studies are available on the vibro-acoustic response of a flat plate with unidirectional stiffeners [40], and no study has been found on bidirectional configurations.

The advantage of the presented method compared to previous work is that the response of both unidirectional and bidirectional-stiffened plate is obtained using only one simple and general matrix formulation. Moreover, both light and heavy fluid effect is included, rendering the method applicable for aircraft and naval stiffened plate designs. In addition, the exact solution for vibro-acoustic responses to a diffuse acoustic field and point force excitation are presented. The predicted results are shown in excellent agreement with FEM and BEM with a significant reduction in computational. However, compared to the latter methods the proposed formulation is limited to flat simply supported panels and neglects direct radiation from the stiffeners.

Section 2 includes a presentation of the analytical solution in predicting the dynamic and acoustic response of finite plates that are evenly and unevenly stiffened with various and eccentric shapes of stiffeners. Section 3 presents a comparison of the predicted results for the dynamic and acoustic response of panels stiffened with varied and eccentrically shaped stiffeners for both unidirectional and bidirectional-stiffened panels with the results obtained using FEM. In Section 4, the predicted transmission loss of stiffened panels are validated using experimental data and a hybrid SEA-periodic model of Cotoni et al. [23] on two flat panels representative of those used in aircraft.

2. Theory

A description of the theoretical model is presented in this section, including the general solution in predicting the vibro-acoustic response of both bidirectionally and unidirectionally stiffened plates.

2.1. General formulations

The flat rectangular panels considered in this study are either unidirectionally or bidirectionally reinforced (Figs. 1 and 2). The plate is assumed to be simply supported and reinforced by N_x and N_y eccentric stiffeners in the x and y directions, respectively, which are either evenly or unevenly spaced along the plate surface. The plate is described using a thin shell theory and the stiffeners are described using Euler–Bernoulli's beam theory. The stiffeners, which are assumed to be physically unconnected to each other, are aligned parallel to the rectangular edge and are fully connected to the plate along their full length. The acoustic radiation from the stiffeners is not taken into account. The effect of fluid loading is, however, accounted for and is shown to be negligible in the studied configurations.

The governing equation of the motion of a thin plate can be written as [28,29] by taking into account the plate's rotational inertia:

$$\tilde{D}_p\nabla^4 W(x,y)-\rho_p h_p\omega^2 W(x,y)-\frac{\rho_p h_p^3\omega^2}{12}\left[\frac{\partial^2 W(x,y)}{\partial x^2}+\frac{\partial^2 W(x,y)}{\partial y^2}\right]=P_{\mathrm{exc}}-\sum_{i=1}^{N_x}F_i^{S_y}\delta(x-x_i)$$
$$-\sum_{i=1}^{N_x}M_i^{S_y}\delta'(x-x_i)-\sum_{j=1}^{N_y}F_j^{S_x}\delta(y-y_j)-\sum_{i=1}^{N_y}M_j^{S_x}\delta'(y-y_j)+P_1+P_2, \quad (1)$$

where $\tilde{D}_p=E_p(1+j\eta)h_p^3/12(1-\nu^2)$ is the plate-bending stiffness. E_p, h_p, ν_p, ρ_p and η are, respectively, Young's modulus, thickness, Poisson's ratio, density and damping coefficient of the plate. $F_j^{S_x}$, $F_i^{S_y}$ are the transverse shear force in x and y at positions x_i and y_j. $M_j^{S_x}$; $M_i^{S_y}$ are the moment per unit length at the ith and jth stiffener–plate interface. P_{exc} and P_l $\{l=1, 2\}$ are the external excitation and fluid loading pressures. δ and δ' represent dirac operators and its spatial derivative, respectively.

The governing equations of the flexural and torsional displacements of the ith and jth stiffener in the y-direction and the x-direction are given by

$$E_{x_i}I_{x_i}\frac{\partial^4 U^i_{S_y}(y)}{\partial y^4}-\rho_{x_i}A_{x_i}\omega^2 U^i_{S_y}(y)=F_i^{S_y}, \quad (2)$$

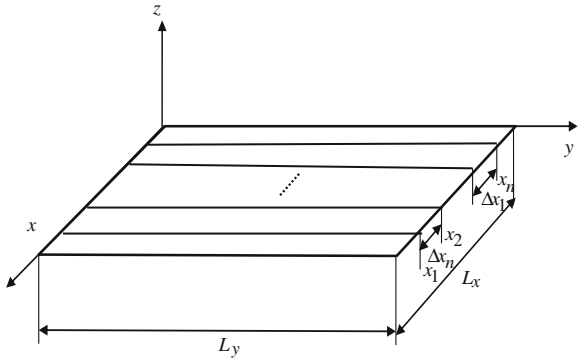

Fig. 1. Unidirectionally stiffened plate.

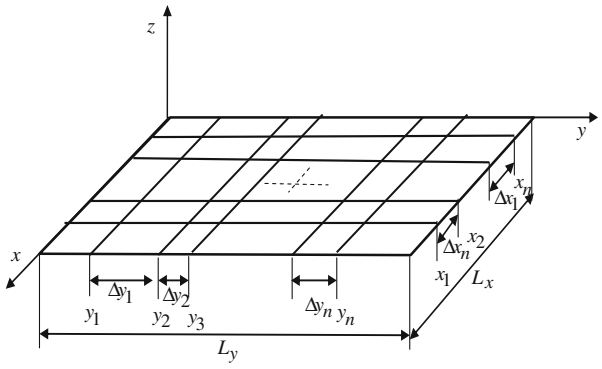

Fig. 2. Bidirectionally stiffened plate.

$$G_{x_i}J_{x_i}\frac{\partial^2\theta^i_{S_y}(y)}{\partial y^2}-\rho_{x_i}I_{p_{x_i}}\omega^2\theta^i_{S_y}(y)=M_i^{S_y}, \tag{3}$$

$$E_{y_j}I_{y_j}\frac{\partial^4U^j_{S_x}(x)}{\partial x^4}-\rho_{y_j}A_{y_j}\omega^2U^j_{S_x}(x)=F_j^{S_x}, \tag{4}$$

$$G_{y_j}J_{y_j}\frac{\partial^2\theta^j_{S_x}(x)}{\partial x^2}-\rho_{y_j}I_{p_{y_j}}\omega^2\theta^j_{S_x}(x)=M_j^{S_x}, \tag{5}$$

where $U^i_{S_x}$, $U^j_{S_y}$ are transversal displacement at the joint lines of attachments and $\theta^i_{S_x}$, $\theta^j_{S_y}$ are torsional angles. $E_{x_i}I_{x_i}$, $E_{x_j}I_{x_j}$ are the bending rigidities and $G_{x_i}J_{x_i}$, $G_{y_j}J_{y_j}$ are the torsional rigidities of the stiffeners in the "x-wise and y-wise" directions, respectively. ρ_{x_i}, ρ_{y_j} and A_{x_i}, A_{y_j} are the mass and surface of the stiffener, I_{x_i}, I_{y_j} and $I_{p_{x_i}}$, $I_{p_{y_j}}$ are the moment of the inertia and the polar moment of inertia of the stiffener cross section about its center of mass, respectively. Damping is included using complex elasticity coefficients. To account for eccentricity between the neutral axis of the stiffeners and the mid-plane of the plate, Huygens' formula [38] is used to calculate the moment of inertia of the stiffeners about the mid-plane of the plate.

The compatibility conditions at the beam/plate interfaces read:

$$U^i_{S_y}(y)=W(x_i,y), \tag{6}$$

$$\theta^i_{S_y}(y)=\frac{\partial W(x_i,y)}{\partial x}, \tag{7}$$

$$U^j_{S_x}(x)=W(x,y_j), \tag{8}$$

$$\theta^j_{S_x}(x)=\frac{\partial W(x,y_j)}{\partial y}. \tag{9}$$

Eqs. (1)–(5) are solved by modal expansion of the displacement fields of the plate and stiffeners:

$$W(x,y)=\sum_m\sum_n W_{mn}\varphi_m(x)\varphi_n(y), \tag{10}$$

$$U^i_{S_y}(y)=\sum_n U^i_n\varphi_n(y), \tag{11}$$

$$\theta^i_{S_y}(y)=\sum_n \theta^i_n\varphi_n(y), \tag{12}$$

$$U^i_{S_x}(x)=\sum_m U^j_m\varphi_m(x), \tag{13}$$

$$\theta^j_{S_x}(y)=\sum_m \theta^j_m\varphi_m(x). \tag{14}$$

where $\varphi_m(x)=\sin(m\pi x/L_x)$ and $\varphi_n(y)=\sin(n\pi y/L_y)$ are the mode shape (trial functions) for simply supported boundary conditions. W_{mn}, U^i_n, θ^i_n are the modal coefficients of the (m, n)th bending mode and modal coefficient of nth flexural and torsional mode of the ith beam, respectively.

Multiplying Eq. (1) and Eqs. (2)–(5) by their respective mode shape functions and integrating each along the surface of the skin and along the length of stiffener, respectively, leads to

$$Z^s_{mn}W_{mn}=P_{mn}-\sum_i^{N_x}F^{S_y}_{ni}\varphi_m(x_i)-\sum_i^{N_x}M^{S_y}_{ni}\varphi'_m(x_i)-\sum_j^{N_y}F^{S_x}_{mj}\varphi_n(y_j)-\sum_j^{N_y}M^{S_y}_{mj}\varphi'_n(y_j)+j\omega\sum_p\sum_q Z_{pqmn}W_{pq}, \tag{15}$$

where $Z^s_{mn}=\rho h_p\left(\frac{D_p}{\rho h_p}k^4_{mn}-\omega^2-\omega^2\frac{h_p^2}{12}(k_m^2+k_n^2)\right)N_{mn}$ is the structural impedance with $N_{mn}=L_xL_y/4$, and Z_{pqmn} is the radiation impedance. $k_{mn}=\sqrt{k_m^2+k_n^2}$ is the modal wavenumber of the (m, n)th plate-bending mode where the terms $k_m=m\pi/L_x$ and $k_n=n\pi/L_y$ are the modal wavenumber components of the rectangular plate with respect to the two orthogonal plate edge

directions. Eq. (15) can be written explicitly as

$$\begin{bmatrix} Z_{11s}-j\omega Z_{1111} & Z_{1211} & \cdots & Z_{m\_\max\, n\_\max 11} \\ Z_{1112} & Z_{12s}-j\omega Z_{1212} & \cdots & Z_{m\_\max\, n\_\max 12} \\ \vdots & \vdots & \vdots & \vdots \\ Z_{11m\_\max\, n\_\max} & \cdots & \cdots & Z^{S}_{m\_\max\, n\_\max\, m\_\max\, n\_\max}-j\omega Z_{m\_\max\, n\_\max\, m\_\max\, n\_\max} \end{bmatrix} \begin{bmatrix} W_{11} \\ W_{12} \\ \vdots \\ W_{m\_\max\, n\_\max} \end{bmatrix}$$

$$= \begin{bmatrix} P_{11}-\sum_{i}^{N_x} F^{S_y}_{1i}\varphi_1(x_i)-\sum_{i}^{N_x} M^{S_y}_{1i}\varphi'_1(x_i)-\sum_{j}^{N_y} F^{S_x}_{1j}\varphi_1(y_j)-\sum_{j}^{N_y} M^{S_y}_{1j}\varphi'_1(y_j) \\ P_{12}-\sum_{i}^{N_x} F^{S_y}_{2i}\varphi_1(x_i)-\sum_{i}^{N_x} M^{S_y}_{2i}\varphi'_1(x_i)-\sum_{j}^{N_y} F^{S_x}_{1j}\varphi_2(y_j)-\sum_{j}^{N_y} M^{S_y}_{1j}\varphi'_2(y_j) \\ \vdots \\ P_{m\_\max n\_\max}-\sum_{i}^{N_x} F^{S_y}_{n\_\max\, i}\varphi_{m\_\max}(x_i)-\sum_{i}^{N_x} M^{S_y}_{n\_\max\, i}\varphi'_{m\_\max}(x_i)\sum_{j}^{N_y} F^{S_x}_{m\_\max j}\varphi_{n\_\max}(y_j)-\sum_{j}^{N_y} M^{S_y}_{m\_\max j}\varphi'_{n\_\max}(y_j) \end{bmatrix}, \tag{16}$$

where m_max, n_max are the selected truncation orders for the mode shape functions. The solution for Eq. (16) has the following form:

$$W_{mn}=\sum_p\sum_q A_{mnpq}\left[P_{pq}-\sum_{i=1}^{N_x} F^{S_y}_{qi}\varphi_p(x_i)-\sum_{i=1}^{N_x} M^{S_y}_{qi}\varphi'_p(x_i)-\sum_{j=1}^{N_y} F^{S_x}_{pj}\varphi_q(y_j)-\sum_{j=1}^{N_y} M^{S_x}_{pj}\varphi'_q(y_j)\right], \tag{17}$$

where A_{pqmn} are the coefficients of the admittance matrix obtained from the inversion of the impedance matrix of Eq. (16).

The expression of the transversal and rotational modal coefficients is given by

$$U^i_n=\frac{F^{S_y}_{ni}}{Z_{ni}}, \tag{18}$$

$$\theta^i_n=\frac{M^{S_y}_{ni}}{Z_{Tni}}, \tag{19}$$

$$U^j_m=\frac{F^{S_x}_{mi}}{Z_{mj}}, \tag{20}$$

$$\theta^j_m=\frac{M^{S_x}_{mi}}{Z_{Tmj}}, \tag{21}$$

where $Z_{ni}=N_n(E_{x_i}I_{x_i}k_n^2-\rho_{x_i}I_{x_i}\omega^2)$ with N_n=L_y/2, $Z_{Tni}=N_n(G_{x_i}J_{x_i}k_n^2-\rho_{x_i}I_{p_{x_i}}\omega^2)$, $Z_{mj}=N_m(E_{y_j}I_{y_j}k_m^2-\rho_{y_j}I_{y_j}\omega^2)$ with N_m=L_x/2, $Z_{Tmj}=N_m(G_{y_j}J_{y_j}k_m^2-\rho_{y_j}I_{p_{yj}}\omega^2)$, $P_{mn}=\iint_S P_{exc}\varphi_m(x)\varphi_n(y)\,dx\,dy$, $F^{S_y}_{ni}=\int_y F^{S_y}_i\varphi_n(y)\,dy$, $M^{S_y}_{ni}=\int_y M^{S_y}_i\varphi_n(y)\,dy$, $F^{S_x}_{mj}=\int_x F^{S_x}_j\varphi_m(x)\,dx$, $M^{S_x}_{mj}=\int_x M^{S_x}_j\varphi_m(x)\,dx$, $\varphi'_n(y)=\partial\varphi_n(y)/\partial y$, $\varphi'_m(x)=\partial\varphi_m(x)/\partial x$.

Using the compatibility conditions in Eqs. (6)–(9) and Eqs. (17)–(21), we obtain the expression of modal displacement vector{W}at each frequency:

$$\{W\}=[A]\left[\{P\}-[\psi][\phi]^{-1}[H]^T\right], \tag{22}$$

where ^{T} denotes the matrix transpose, $[A]$ is the admittance matrix and $\{P\}$ is the vector of the modal load. The components of matrices $[\phi]$, $[\psi]$ and vector $\{H\}$ are given in Appendix A.

After a few algebraic manipulations, we obtain the following expression for the plate's modal displacements:

$$W_{mn}=\sum_p\sum_q A_{pqmn}\left[P_{pq}-\sum_{k}^{m\_\max}\sum_{l}^{n\_\max}\sum_{i}^{N_x} P_{kl}\alpha^i_k-\sum_{k'}^{m\_\max}\sum_{l'}^{n\_\max}\sum_{j}^{N_y} P_{k'l'}\beta^j_{k'l'}\right], \tag{23}$$

where α^i_k and $\beta^i_{k'l'}$ are complex parameters given in Appendix A.

Expression (23) is a general expression allowing the prediction of the modal displacement in both light and heavy fluids. In the case of light-fluid loading, the modal displacement can be simplified by cancelling the cross-modal terms:

$$W_{mn}=\frac{1}{Z^s_{mn}-j\omega Z_{mnmn}}\left[P_{mn}-\sum_k\sum_l\sum_i^{N_x} P_{kl}\alpha^i_{kl}-\sum_k\sum_l\sum_i^{N_y} P_{k'l'}\beta^j_{k'l'}\right]. \tag{24}$$

The fluid impedance Z_{mnmn} can be written as

$$Z_{mnmn}=R_{mnmn}+jX_{mnmn}. \tag{25}$$

In the case of light fluid the radiation reactance X_{mnmn} can also be neglected compared to the radiation resistance R_{mnmn}. The latter is given by

$$R_{mnmn} = \rho_0 c_0 \sigma_{mn} \delta_{mn}, \tag{26}$$

where ρ_0 and c_0 are the density and speed of the fluid, and σ_{mn} is the modal radiation efficiency. In this study, we obtained it using Leppington's asymptotic formulas [30].

2.1.1. Response to point force excitation

Considering the model of a plate with eccentric and regular or irregular inter-rib stiffeners, attached along the "x-wise and y-wise directions". Excited by a point force P_0 at an arbitrary point (x_0, y_0), the classical vibration indicators of the plate are easily derived. The space-averaged quadratic velocity and the quadratic velocity itself are given by

$$\langle V^2(\omega)\rangle = \frac{\omega^2}{8}\sum_m\sum_n |W_{mn}|^2, \tag{27}$$

where W_{mn} is given by Eq. (23) or (24) and P_{mn} is provided in the following expression:

$$P_{mn} = P_0 \varphi_m(x_0)\varphi_n(y_0). \tag{28}$$

The radiated power can be written as follows:

$$\Pi_r(\omega) = \frac{\omega^2}{2}\Re\{W\}^T[Z]\{W\}, \tag{29}$$

where $[Z]$ is the radiation impedance matrix and $\Re$ denotes the real part.

2.1.2. Response to diffuse field, point force and turbulent boundary layer load

For a diffuse acoustic field excitation, the vibro-acoustic responses are obtained by considering a plane wave excitation having incidences angles φ, θ about the x-axis and z-axis, respectively. The quadratic velocity is given by

$$\begin{aligned}\langle V^2(\varphi,\theta,\omega)\rangle &= \frac{\omega^2}{8}\sum_m\sum_n |W_{mn}(\varphi,\theta,\omega)|^2\\
&= \frac{\omega^2}{8}\sum_m\sum_n\sum_p\sum_q\sum_{p'}\sum_{q'} A_{mnpq}\left(A_{mnp'q'}\right)^*\left((P_{pq})(P_{p'q'})^* + \left(\sum_k^{m_max}\sum_l^{n_max}\sum_i^{N_x} P_{kl}\alpha_k^i\right)\left(\sum_k^{m_max}\sum_l^{n_max}\sum_i^{N_x} P_{kl}\alpha_k^i\right)^*\right.\\
&\quad + \left(\sum_{k'}^{m_max}\sum_{l'}^{n_max}\sum_j^{N_y} P_{k'l'}\beta_{k'l'}^j\right)\left(\sum_{k'}^{m_max}\sum_{l'}^{n_max}\sum_j^{N_y} P_{k'l'}\beta_{k'l'}^j\right)^* - 2\Re\left\{(P_{pq})\left(\sum_k^{m_max}\sum_l^{n_max}\sum_i^{N_x} P_{kl}\alpha_k^i\right)^*\right\}\\
&\quad \left. - 2\Re\left\{(P_{pq})\left(\sum_{k'}^{m_max}\sum_{l'}^{n_max}\sum_j^{N_y} P_{k'l'}\beta_{k'l'}^j\right)^*\right\} - 2\Re\left\{\left(\sum_k^{m_max}\sum_l^{n_max}\sum_i^{N_x} P_{kl}\alpha_k^i\right)\left(\sum_{k'}^{m_max}\sum_{l'}^{n_max}\sum_j^{N_y} P_{k'l'}\beta_{k'l'}^j\right)^*\right\}\right),\end{aligned} \tag{30}$$

where * denotes the conjugate.

By assuming that the fluid is light, the contribution of cross-modal loading terms $(P_{mn}P_{pq}^*)$ and the cross-modal terms of the radiation impedance are negligible and the quadratic velocity of the stiffened plate can be written as

$$\begin{aligned}\langle V^2(\varphi,\theta,\omega)\rangle = \frac{\omega^2}{8}\sum_m\sum_n \frac{1}{|Z_{mn}^s - j\omega Z_{mnmn}|^2}&\left(|P_{mn}(\varphi,\theta,\omega)|^2 + \sum_k\sum_l |P_{kl}(\varphi,\theta,\omega)|^2\left|\sum_{i=1}^{N_x}\alpha_{kl}^i\right|^2\right.\\
&+ \sum_k\sum_l |P_{kl}(\varphi,\theta,\omega)|^2\left|\sum_{j=1}^{N_y}\beta_{kl}^j\right|^2 - 2|P_{mn}(\varphi,\theta,\omega)|^2\Re\left\{\sum_{j=1}^{N_y}\beta_{mn}^j\right\}\\
&\left. - 2|P_{mn}(\varphi,\theta,\omega)|^2\Re\left\{\sum_{i=1}^{N_x}\alpha_{mn}^i\right\} - 2\sum_k\sum_l |P_{kl}(\varphi,\theta,\omega)|^2\Re\left\{\left(\sum_{i=1}^{N_x}\alpha_{kl}^i\right)^*\left(\sum_{j=1}^{N_y}\beta_{kl}^j\right)\right\}\right).\end{aligned} \tag{31}$$

The expression of the modal loading terms $|P_{mn}(\varphi,\theta,\omega)|^2$ is computed using Maidanik's formulation [24].

The quadratic velocity for a diffuse acoustic field is obtained by averaging over all incident angles:

$$\langle V^2(\omega)\rangle = \int_0^{2\pi}\int_0^{\theta_{\max}} \langle V^2(\varphi,\theta,\omega)\rangle \sin(\theta)\cos(\theta)\, d\theta\, d\varphi. \tag{32}$$

This leads to

$$\langle V^2(\omega)\rangle = \frac{\omega^2}{8}\sum_m\sum_n \frac{1}{|Z_{mn}^s - j\omega Z_{mnmn}|^2}\left(J_{mn}^2 + \sum_k\sum_l J_{kl}^2\left|\sum_{i=1}^{N_x}\alpha_{kl}^i\right|^2 + \sum_k\sum_l J_{kl}^2\left|\sum_{j=1}^{N_y}\beta_{kl}^j\right|^2\right.$$

$$-2J_{mn}^2\,\Re\left\{\sum_{i=1}^{N_x}\alpha_{mn}^i\right\}-2J_{mn}^2\,\Re\left\{\sum_{j=1}^{N_y}\beta_{mn}^j\right\}-2\sum_k\sum_l J_{kl}^2\,\Re\left\{\left(\sum_{i=1}^{N_x}\alpha_{kl}^i\right)^*\left(\sum_{j=1}^{N_y}\beta_{kl}^j\right)\right\}\Bigg), \tag{33}$$

where $J_{mn}^2(\omega)$ is the joint acceptance in a diffuse field given by

$$J_{mn}^2(\omega)=\int_0^{2\pi}\int_0^{\theta_{\max}}|P_{mn}(\varphi,\theta,\omega)|^2\sin(\theta)\cos(\theta)\,d\theta\,d\varphi \tag{34}$$

and $\theta_{\max}$ is the maximum angle of incidence.

The remaining integration in Eq. (34) is difficult to perform analytically, but due to the nature of the integrand, it lends itself easily to numerical integration.

The radiated power in a diffuse field can be written as

$$\Pi_r(\omega)=\frac{\omega^2}{2}\,\Re\sum_m\sum_n\frac{Z_{mnmn}}{|Z_{mn}^s-j\omega Z_{mnmn}|^2}\left(J_{mn}^2+\sum_k\sum_l J_{kl}^2\left|\sum_{i=1}^{N_x}\alpha_{kl}^i\right|^2+\sum_k\sum_l J_{kl}^2\left|\sum_{j=1}^{N_y}\beta_{kl}^j\right|^2\right.$$
$$\left.-2J_{mn}^2\,\Re\left\{\sum_{i=1}^{N_x}\alpha_{mn}^i\right\}-2J_{mn}^2\,\Re\left\{\sum_{j=1}^{N_y}\beta_{mn}^j\right\}-2\sum_k\sum_l J_{kl}^2\,\Re\left\{\left(\sum_{i=1}^{N_x}\alpha_{kl}^i\right)^*\left(\sum_{j=1}^{N_y}\beta_{kl}^j\right)\right\}\right)\delta_{mn}. \tag{35}$$

The transmission loss is given by

$$TL=10Log(1/\tau(\omega)), \tag{36}$$

where $\tau(\omega)$ is the transmission coefficient in a diffuse field that is obtained by averaging overall incidence angles:

$$\tau(\omega)=\frac{\int_0^{2\pi}\int_0^{\theta_{\max}}\Pi_r(\varphi,\theta,\omega)/\Pi_i(\varphi,\theta,\omega)\sin(\theta)\cos(\theta)\,d\varphi\,d\theta}{\int_0^{2\pi}\int_0^{\theta_{\max}}\sin(\theta)\cos(\theta)\,d\varphi\,d\theta}. \tag{37}$$

The incident power is given by

$$\Pi_i(\varphi,\theta,\omega)=\frac{\cos(\theta)S}{2\rho_0c_0}, \tag{38}$$

$$TL=-10Log_{10}\left\{\frac{\rho_0c_0\omega^2}{\pi S}\,\Re\sum_m\sum_n\frac{Z_{mnmn}}{|Z_{mn}^s-j\omega Z_{mnmn}|^2}\left(T_{mn}^2+\sum_k\sum_l T_{kl}^2\left|\sum_{i=1}^{N_x}\alpha_{kl}^i\right|^2+\sum_k\sum_l T_{kl}^2\left|\sum_{j=1}^{N_y}\beta_{kl}^j\right|^2\right.\right.$$
$$\left.\left.-2T_{mn}^2\,\Re\left\{\sum_{i=1}^{N_x}\alpha_{mn}^i\right\}-2J_{mn}^2\,\Re\left\{\sum_{j=1}^{N_y}\beta_{mn}^j\right\}-2\sum_k\sum_l T_{kl}^2\,\Re\left(\sum_{i=1}^{N_x}\alpha_{kl}^i\right)^*\left(\sum_{j=1}^{N_y}\beta_{kl}^j\right)\right)\delta_{mn}\right\}. \tag{39}$$

The expression of T_{mn}^2 is given by

$$T_{mn}^2=\int_0^{2\pi}\int_0^{\theta_{\max}}|P_{mn}(\varphi,\theta,\omega)|^2\sin(\theta)\,d\theta\,d\varphi, \tag{40}$$

Note that, when the cross coupling is accounted for, the transmission loss is given using Eqs. (23), (29), (37) and (38). This will include the average of the cross-modal loading terms given by [44]

$$\int_0^{2\pi}\int_0^{\pi}P_{mn}(\varphi,\theta,\omega)P_{pq}^*(\varphi,\theta,\omega)\sin(\theta)\,d\theta\,d\varphi=\frac{16\pi^2R_{mnpq}}{\rho_0c_0Sk_0^2}, \tag{41}$$

where $k_0$is the acoustic wave number, and S is the surface of the skin.

For a TBL excitation, the quadratic velocity and radiated power are given by Eqs. (33) and (35), respectively, with the joint acceptance J_{mn}^2 given by

$$J_{mn}^2(\omega)=\frac{1}{S^2}\iint_A\iint_{A'}\varphi_m(x')\varphi_n(y')\phi_{pp}(x,y,x',y',\omega)\varphi_m(x)\varphi_n(y)\,dx\,dy\,dx'\,dy', \tag{42}$$

where $\phi_{pp}(x,y,x',y')$ is the spatial power spectral density of blocked parietal pressure of the TBL; by applying Fourier transform in expression (42), the joint acceptance can be written as

$$J_{mn}^2(\omega)=\frac{1}{S^2}\int_{-\infty}^{+\infty}\int_{-\infty}^{+\infty}|S_{pp}(k_x,k_y,\omega)||S_{mn}(k_x,k_y)|\,dk_x\,dk_y, \tag{43}$$

where $S_{pp}(k_x, k_y)$, $S_{mn}(k_x, k_y)$ are respectively the power spectral density of blocked parietal pressure of the TBL and the modal function in the wavenumber domain.

There are many models for the power spectral density of TBL in the literature. Joint acceptance can be performed analytically using Eq. (42) or Eq. (43) for models such as Cockburn's [31], Corcos' [32] and Efimtsov's [33] models, or numerically using Eq. (43) for other models such as Smol'Yakov [42] and Chase models [43].

Finally, it is worth noting that the formulation for unstiffened and unidirectionally stiffened plates is a special case of the previous formulation; their response can be computed by cancelling the sums involving N_x and/or N_x.

3. Numerical results and discussion

We examined the accuracy of the analytical method by comparing the predicted dynamic response to FEM simulations for both unidirectionally and bidirectionally stiffened plates. The shape, inter-rib spacing and eccentricity of the stiffeners were all varied. In the TBL excitation case, the model presented in this study was validated by comparing it to SEA predictions using the commercial software program VAone [34]. This program uses Cockburn's model [32] for the TBL and Bremner's ribbed plate approximation for the ribbed plates [22,41]. For the DAF excitation, the results were validated using an in-house code with NASTRAN for the structural response and Rayleigh's integral for the acoustic response. For the sake of conciseness, the results presented in this section are limited to (i) numerical validations using FEM for a point force excitation and (ii) experimental validation TL prediction. In addition, in all the results presented in this paper, the maximum number of trial functions (base modes of the simple supported plate) is selected by verification of the solution's convergence. This paper does not include a convergence study.

3.1. Plate stiffened unidirectionally

3.1.1. Response to point excitation load on the stiffener

Consider the stiffened plate I shown in Fig. 3a. The cross section of the stiffeners is represented in Fig. 3b. The mechanical and geometrical properties of the plate and the stiffeners are listed in Table 1. The origin of the (x, y) axes is at the lower left corner of the plate. The point force is located on a stiffener at position (0.143 m, 0.11 m).

The predicted quadratic velocity and radiated power from the present model of the stiffened plate with simple eccentric stiffeners is compared with the FEM using the commercial software program MSC.Nastran [35]. In this program, the plate is modeled using Quad4 elements and the stiffeners are modeled as beams (Cbeam elements). Offsets are used to connect the plate and the beams.

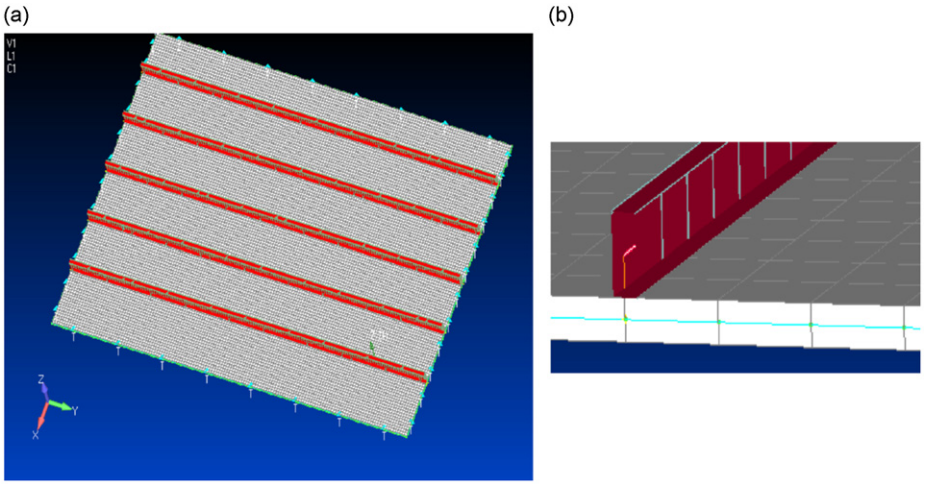

Fig. 3. Unidirectionally stiffened plate: (a) complete structure and (b) stiffener.

Table 1
Properties of unidirectionally stiffened plates.

	Stiffened plate I	Stiffened plate II	Stiffened plate III
Material	Aluminum	Aluminum	Aluminum
Number of stiffeners	$N_x=5$	$N_x=5$	$N_x=5$
Damping	$\eta=0.01$	$\eta=1\%$	$\eta=1\%$
Surface area of skin (m^2)	$S=1.06\times1.54$	$S=1.06\times1.54$	$S=1.06\times1.54$
Thickness of the plate (m)	$hp=8\times10^{-3}$	$hp=8\times10^{-3}$	$h\sim1\times10^{-3}$
Spacing between stiffeners (m)	$S_x=0.18$	$S_x=0.175$	$S_x=0.18$
Moments of inertia of stiffeners (m^4)	$I_{yi}=1.27\times10^{-12}$	$I_{yi}=3.3722\times10^{-8}$	$I_{yi}=7.83\times10^{-9}$
	$I_{zi}=2.93\times10^{-12}$	$I_{zi}=6.0994\times10^{-12}$	$I_{zi}=6.18\times10^{-9}$
Stiffener cross section (m^2)	$A_{yi}=1.52\times10^{-5}$	$A_{yi}=2.68538\times10^{-5}$	$A_{yi}=8.51\times10^{-5}$
Eccentricity (m)	$e_{zz}=1.16\times10^{-3}$	$e_{zz}=1\times10^{-2}$	$e_{zz}=1.642\times10^{-2}$

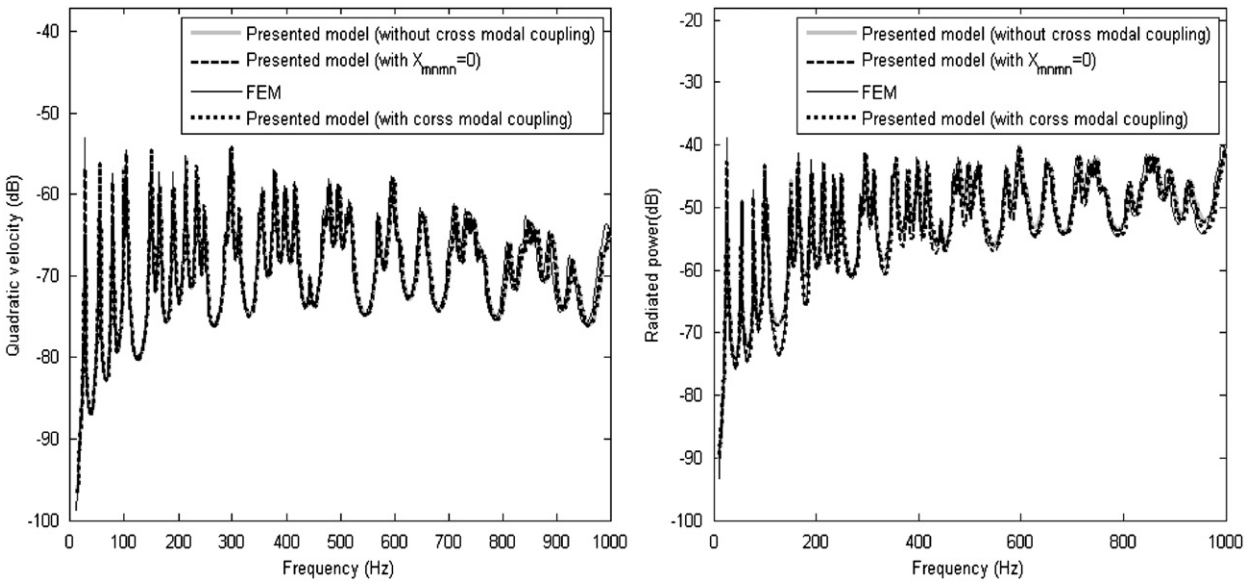

Fig. 4. Comparison of FEM and predicted quadratic velocity and radiated power.

The FEM results are obtained using an in-house code which uses the eigenvalues and the eigenvectors extracted from MSC/NASTRAN. In the FEM model, 7313 CQUAD4 thin shell elements and 514 CBAR beam elements were used. The response was calculated using a modal frequency response analysis in 23 structural modes. In the model presented here, the modal summation is computed using 100 trail functions (summation limited to m_max=10 and n_max=10).

Fig. 4 shows the comparison between predicted and FEM results. Both the space-averaged quadratic velocity and radiated power are predicted by (i) using the full radiation impedance matrix (including the cross-modal terms and reactance terms), (ii) keeping only the diagonal terms of [Z] (light coupling) and (iii) eliminating the imaginary part X_{mnmn} of the radiation impedance. An excellent agreement is obtained for both the space-averaged quadratic velocity and the radiated acoustic power when the cross-modal terms are included in the analysis. However, and as known [37], slight discrepancies are observed between the FEM and predicted results, especially for the radiated power at anti-resonances when the cross-modal terms are neglected. To provide a complete analysis, Fig. 4 also shows the negligible effects when the reactance terms in this light-fluid analysis are included. As well, a slight discrepancy is observed at the first resonances. This may due to the difference between the formulation used to compute the radiation impedance and/or the modal truncation.

On an IBM dual core 2.7 GHz computer with 2 GB of RAM, 504 s of computational time is needed when cross-modal terms are included in the analysis. The time required drops to 244 s when only direct terms are included, compared to 110 s when only the real part of radiation impedance is calculated using Leppington's formulation [30]. The computational time needed for the extraction of modes with the MSC/NASTRAN model on the same machine is 78 s. However, the computational time to predict the vibration and acoustic response using the extracted NASTRAN modes took approximately one hour using a dual-CPU Intel Xeon X5560 quad-core computer, 2.8 GHz of RAM.

3.1.2. Response to point excitation load on the skin

In this example, the stiffened plate II shown in Fig. 5a has eccentric stiffeners with a more complex shape Fig. 5b. Their geometrical properties are listed in Table 1. Moreover, the load is located on the plate at position (0.218 and 0.37379 m) measured from the lower left corner of the plate. The results are shown in Fig. 6.

In FEM predictions, the mesh used in the previous example was conserved. In the analytical predictions, 100 trail functions were used with the cross-modal terms included and 1600 functions with cross-modal terms left out.

Again, Fig. 6 shows slight discrepancies at anti-resonances when the cross-modal terms are neglected and an excellent agreement when the cross-modal terms are included.

The computational cost is the same as in the previous example for the model presented here and the FEM models when a 100 plate mode shape is used. However, the computational time is 1770 s when 1600 trail functions are used. To avoid a long computational time for the radiation impedance and inversion of large matrices, which is dimensionally dependent of the number of plate modes, an exact truncation of the series must be done to obtain an approximate solution with sufficient accuracy.

It is worth noting that at high frequencies such as when the structural wavelength is less than the shortest distance between the point force and the stiffeners, the effect of stiffeners would be negligible and the dynamic response of the stiffened plate similar to the response of the sub-panels between the stiffeners. It is also observed (not shown here) that the stiffened plate has the same response as an equivalent orthotropic plate only at low frequencies. Moreover, there are

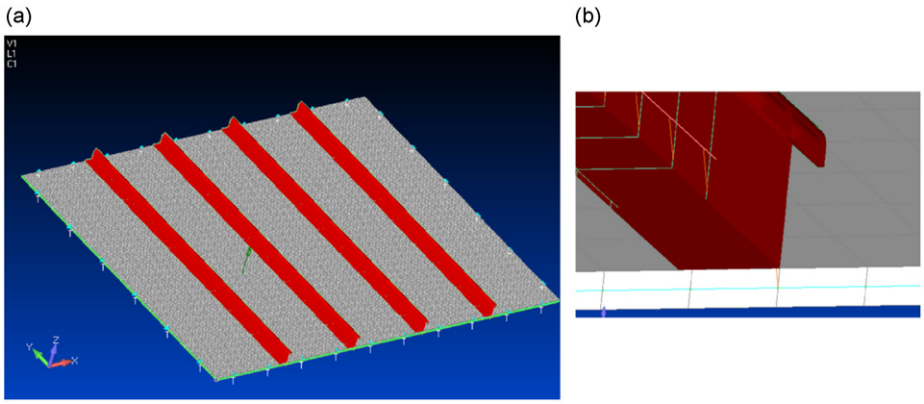

Fig. 5. Unidirectionally stiffened plate: (a) complete structure and (b) stiffener.

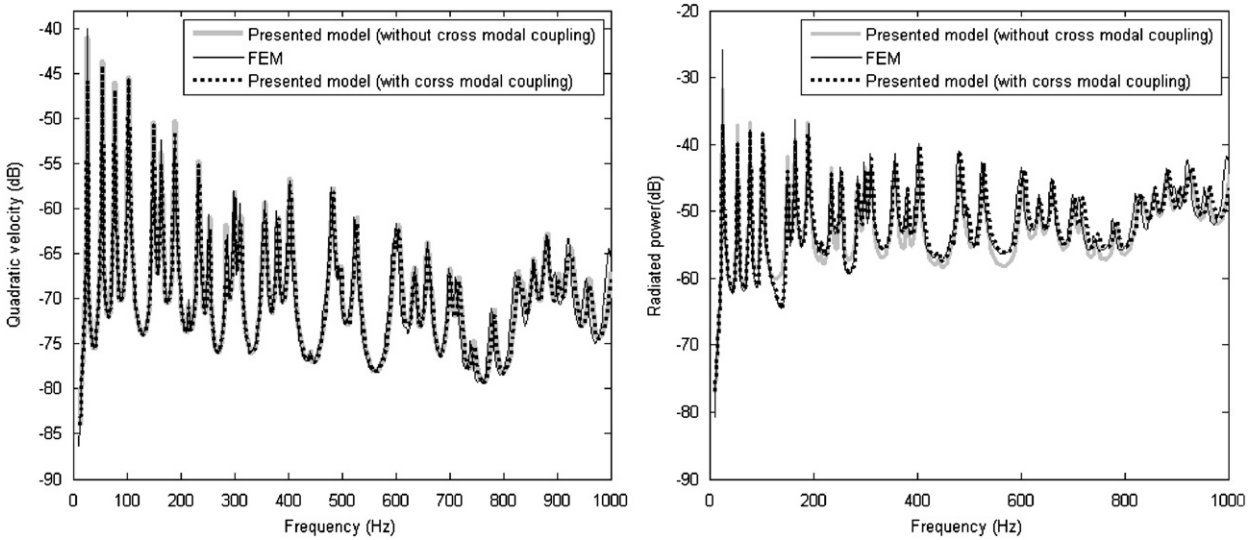

Fig. 6. Comparison of FEM, predicted quadratic velocity and radiated power.

some particular modes of interest at frequencies where the stiffened plate has the same acoustic response as an equivalent unstiffened one as confirmed by Lin [21] in the dynamic response. To illustrate, Fig. 7 shows the overlapping between the acoustics responses of the stiffened and unstiffened plates at frequencies 637, 662 and 703 Hz, corresponding to modes (6,1), (6,2) and (6,3) of the unstiffened plate, respectively. These modes correspond to flexural modes where the plate half-wavelength λ_x along the edge parallel to the x-axis (related to the modal wavenumber $k_x=m\pi/L_x$ by $\lambda_x=2\pi/k_x$) coincides with the spacing between stiffeners S_x: ($n\lambda_x=2S_x$) where n is an integer. This means that all stiffeners are located at nodal locations of these modes. Therefore, the stiffener effect is negligible at these frequencies and the ribbed plate has the same response as an equivalent unstiffened one.

3.2. *Bidirectionally reinforced plates with evenly and unevenly spaced stiffeners*

We studied the evenly and unevenly stiffened plates IV and V shown in Fig. 8a and b, respectively. Table 2 lists the mechanical and geometrical properties of the plates and stiffeners. The point force position on plates IV and V are (0.31 and 0.5 m) and (0.31 and 0.52 m), respectively.

The accuracy of the proposed method was reverified by comparing the predicted space-averaged quadratic velocity and radiated power to FEM results. In the FE model, 7200 CQUAD4 thin shell elements are used for the base plate. The stiffeners are modeled using 420 CBAR beam elements for plate IV and 520 CBAR beam elements for plate V. In the model presented here, the modal summation was computed using 100 base-plate modes. The comparisons are shown in Figs. 9 and 10. Again, the results with and without modal coupling are shown.

The observations are similar to the previous case for both plates IV and V when the cross-modal terms are included or left out in the analysis. The computational time used in the model presented here is 510 s for an evenly stiffened plate and

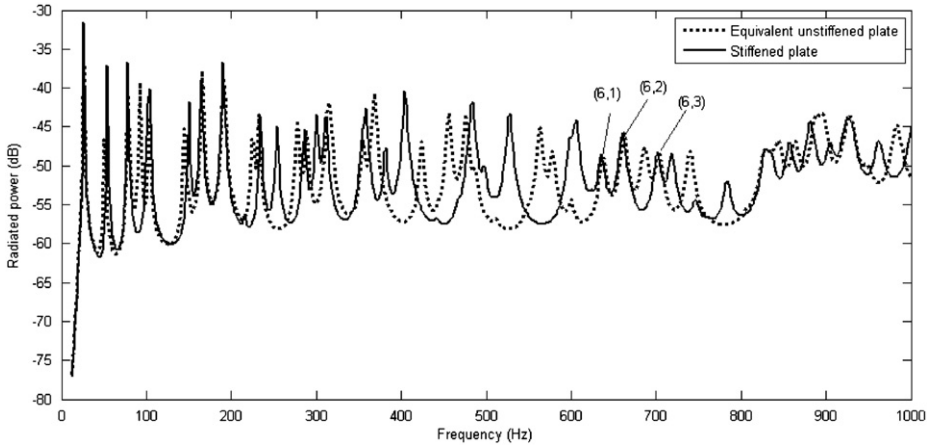

Fig. 7. A comparison between acoustic responses of unidirectionally stiffened plate II and the equivalent unstiffened plate.

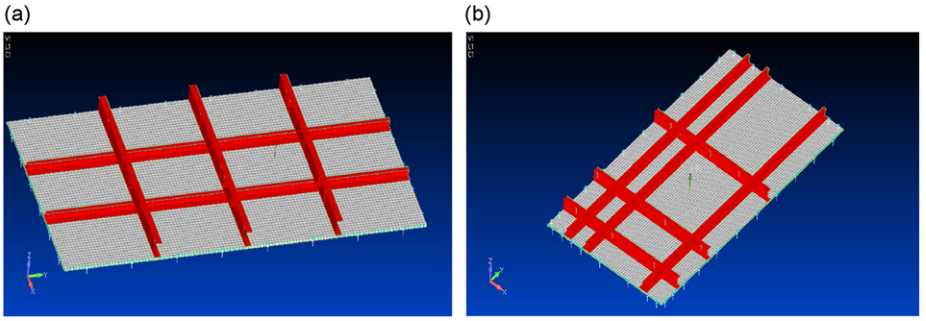

Fig. 8. Bidirectionally stiffened plate: (a) regularly spaced stiffeners and (b) irregularly spaced stiffeners.

Table 2
Properties of bidirectionally stiffened plates.

	Regularly spaced plate IV	Irregularly spaced plate V	Stiffened plate VI
Material	Aluminum	Aluminum	Aluminum
Number of stiffeners	$N_x=2$	$N_x=3$	$N_x=8$
	$N_y=3$	$N_y=3$	$N_y=5$
Damping	$\eta=1\%$	$\eta=1\%$	$\eta=1\%$
Surface area of skin (m^2)	$S=0.6\times1.2$	$S=0.6\times1.2$	$S=1.3716\times1.6256$
Thickness of the plate (m)	$hp=8\times10^{-3}$	$hp=8\times10^{-3}$	hp~1×10^{-3}
Spacing between stiffeners (m)	$S_x=0.2$	$S_{x1}=0.1$; $S_{x2}=0.3$	$S_x=0.175$
	$S_y=0.3$	$S_{y1}=0.2$; $S_{y2}=0.4$	$S_{yi}=0.375$
Moments of inertia of stiffeners (m^4)	$I_{xi}=2.0738\times10^{-12}$	$I_{xi}=2.0738\times10^{-12}$	$I_{xi}=8.71\times10^{-8}$
	$I_{yi}=9.3184\times10^{-9}$	$I_{yi}=9.3184\times10^{-9}$	$I_{yi}=5.47\times10^{-9}$
Stiffener cross section (m^2)	$A_{xi}=2.112\times10^{-5}$	$A_{xi}=2.112\times10^{-5}$	$A_{xi}=1.13\times10^{-4}$
	$A_{yi}=2\times10^{-5}$	$A_{yi}=2\times10^{-5}$	$A_{yi}=8.99\times10^{-5}$
Eccentricity (m)	$e_{zz\_x}=10^{-2}$	$e_{zz\_x}=10^{-2}$	$e_{zz\_x}=3.95\times10^{-2}$
	$e_{zz\_y}=1.4\times10^{-2}$	$e_{zz\_y}=1.4\times10^{-2}$	$e_{zz\_y}=1.67955\times10^{-2}$

700 s for an unevenly stiffened plate when the cross-modal terms are included. The time needed by MSC/NASTRAN for the extraction of modes on the same machine is 55 and 70 s for even and uneven plate stiffening, respectively. The time needed by the in-house code is more than one hour in both cases, using the same Intel Xeon X5560 computer.

4. Experimental validation

This section presents the experimental validation for the prediction of transmission loss of the two stiffened panels. The first panel (III) (Table 1) has unidirectional stiffeners and the second panel (VI) (Table 2) has orthogonal stiffeners. The experimental measurements presented here were carried out at the Université de Sherbrooke.

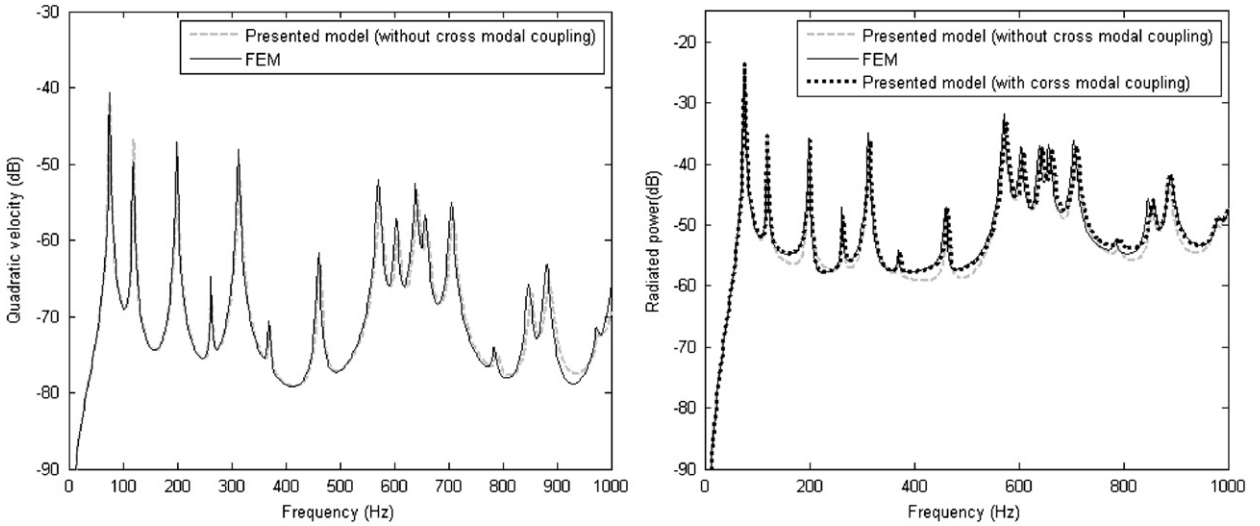

Fig. 9. Comparison of FEM and predicted quadratic velocity and radiated power of regularly spaced stiffeners on plate IV.

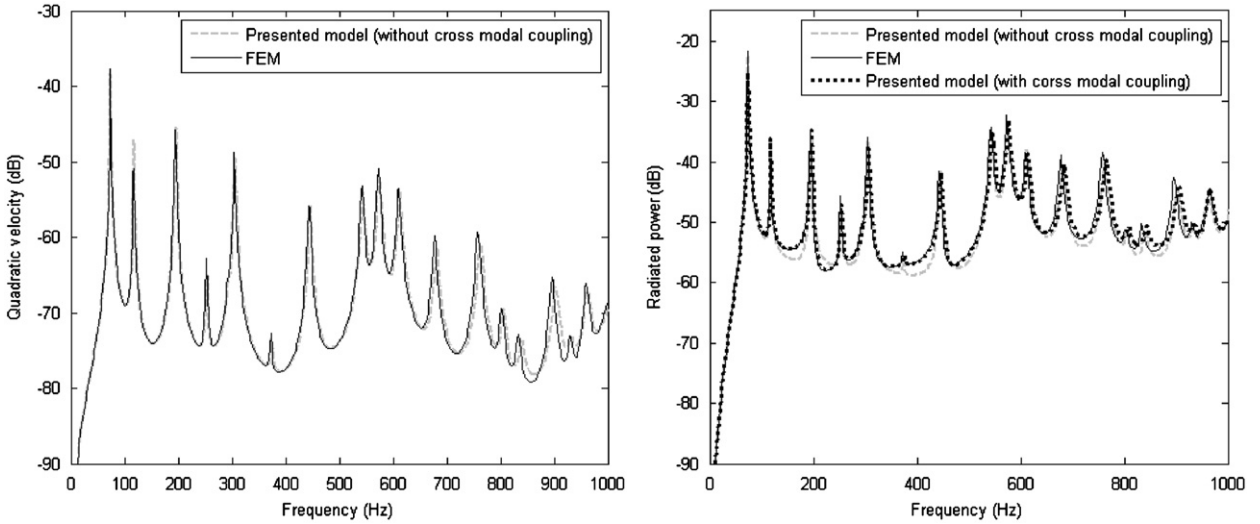

Fig. 10. Comparison of FEM and predicted quadratic velocity and radiated power of the irregularly spaced stiffeners on plate V.

4.1. Transmission loss on a unidirectionally stiffened plate loaded by diffuse field

The stiffened panel (III) was mounted between a reverberation room and an anechoic room and its TL was measured according to standard ISO 15186-1: 2000. The low frequency limit of the used transmission loss facility is around 200 Hz (reverberation room volume equal to 143 m^3).

The comparison between measurement and predicted transmission loss of the stiffened panel (III) is shown in Fig. 11. The field incidence (θ_{max}=78°) is used in the predictions. Overall, the comparison is good. Note in particular that the presented method is able to predict the dips at 315 and 1250 Hz. However, these dips are less pronounced in the experiments.

Using presented model or directly the NASTRAN model, one can visualize the modes of the panel to estimate the wavelength (structural trace) of the plate at each frequency. In this example, it is found that below 98 Hz the behavior is controlled by global modes. The first sub-panel mode is at approximately 100 Hz and its effect is not clearly seen in the TL curve. The dips observed at 315 Hz, and 1250H 1/3-octave bands were correlated with high-order sub-panel modes localized at one edge of the panel (the local modes are highly attenuated in the other sub-panels).

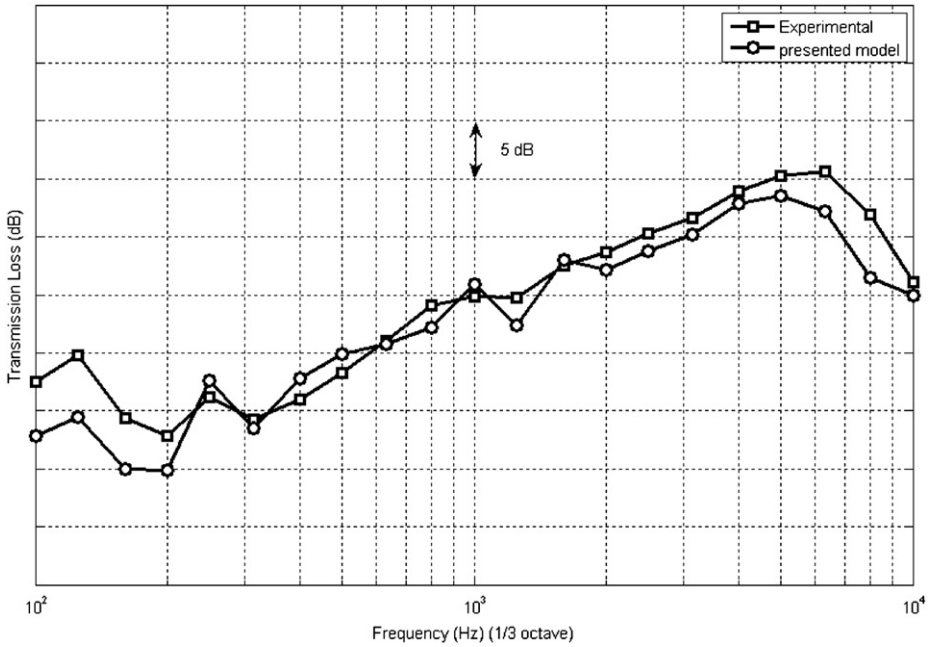

Fig. 11. Comparison between predicted and test measurement of transmission loss.

Fig. 12. Pictures of the orthogonally ribbed panel mounted between the reverberant and anechoic rooms; seen from the excitation room (left) and the receiver room (right).

The discrepancy observed at low frequencies may be due to boundary conditions. In fact, the model assumes simple support while in the test the panel edges were sandwiched between two decoupled flat bars using a neoprene seal. The boundary conditions are somehow closer to clamping than simple support; however, no attempt was made to identify the test boundary conditions. Moreover, the size of the used reverberation room limits the lowest frequency range to 200 Hz and thus the results at 100 and 160 Hz may be questionable.

The discrepancies at higher frequencies, near the critical frequency of the base plate, are certainly due to damping. In the simulation, a constant 1% structural damping was used for both the plate and the stiffeners. Better agreement could have been achieved if damping had been measured (edge damping) and used in the simulations.

4.2. Transmission loss of bidirectionally stiffened plate loaded by a diffuse field

In this test case, the measurement was conducted on a bidirectionally stiffened panel. Fig. 12 shows pictures of the stiffened panel (VI) as mounted in the transmission loss facility.

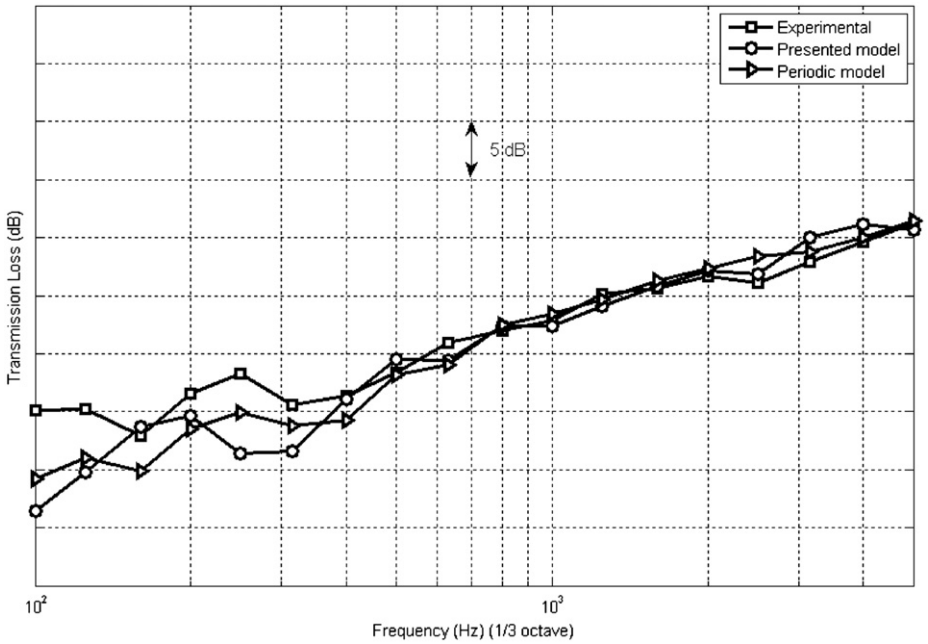

Fig. 13. Comparison between predicted, measured and periodic model results for transmission loss.

Fig. 13 shows the comparison between prediction and measurement. Results from the hybrid SEA–FE periodic model presented by Cotoni et al. [23] are also shown. The commercial software VAone [35] was used to compute these results. Field incidence was used in the predictions both the presented model and the hybrid model are able to accurately capture the measured TL. Both models predict the dip at 315 Hz. This dip are again highly damped in the experiment, which is certainly related to edge damping (neoprene was used to attach the panel in the mounting window). The discrepancies below 315 Hz are due to boundary conditions.

Based on the Bremner [22] model it is observed that low frequencies are governed by global modes and medium and high frequencies are governed by periodic and local modes. This transition between the modes produces an increase of sound transmission, due to the large radiation efficiency of the smaller size panels (sub-panels) at the so-called frequency of transition. Therefore, the dip observed on the TL in the 315 Hz 1/3-octave band may be due to the transition between global and local modes.

5. Conclusion

This paper presented a simple semi-analytical model employing the modal expansion technique in order to predict the vibro-acoustic response of finite ribbed panels under various excitations. Both unidirectionally and bidirectionally stiffened panels were implemented. The effects of stiffener shape, position and eccentricity were considered along with a clear analysis of the effect of cross-modal coupling. Regularly and irregularly stiffened plates with various eccentricities and stiffener cross-sections were studied to validate the accuracy of the analytical method in comparison with the FEM for vibration and BEM (Rayleigh's integral) for sound radiation. Transmission loss tests were also conducted to validate the model in comparison with a hybrid SEA/FEM periodic model. The presented model agrees very well with experimental tests in most frequency ranges of interest. In all studied configurations, a reduction in computational cost (CPU time and memory) was achieved in comparison with the finite element and Boundary element method. The results of the simulations and tests corroborate the classical behavior of stiffened panels. Although limited to a simple geometry (flat panel) and simple boundary conditions (simple support) compared to FEM/BEM based methods, the present model still represents an excellent tool for quick and accurate parametric studies. One other particular application of the presented model is the quick estimation of the modal density and radiation efficiency of stiffened panels for SEA applications [39].

Acknowledgment

The authors thank NSERC (National Sciences and Engineering Research Council of Canada) industrial research chair in aviation acoustics for its financial support.

Appendix A. Matrices component for the bidirectionally stiffened plate

In Eq. (22), the matrix $[\phi]$ is to be inverted numerically. This matrix is square and frequency dependent with dimensions of $(2N_x n\_\max+2N_y m\_\max)$.[2] The general form of this matrix, taking into account the cross-modal terms, is given by

$$[\phi]=\left[\begin{array}{ccc|ccc|ccc|ccc}
[\mathbf{A}_1^1] & \dots & [\mathbf{A}_1^{Nx}] & [\mathbf{C}_1^1] & \dots & [\mathbf{C}_1^{Nx}] & [\mathbf{E}_1^1] & \dots & [\mathbf{E}_1^{Ny}] & [\mathbf{F}_1^1] & \dots & [\mathbf{F}_1^{Ny}] \\
\vdots & \vdots & \vdots & \vdots & \vdots & \vdots & \vdots & \vdots & \vdots & \vdots & \vdots & \vdots \\
[\mathbf{A}_{N_x}^1] & \dots & [\mathbf{A}_{N_x}^{N_x}] & [\mathbf{C}_{N_x}^1] & \dots & [\mathbf{C}_{N_x}^{N_x}] & [\mathbf{E}_{N_x}^1] & \dots & [\mathbf{E}_{N_x}^{N_y}] & [\mathbf{F}_{N_x}^1] & \dots & [\mathbf{F}_{N_x}^{N_y}] \\
\hline
[\mathbf{C}_1^1] & \dots & [\mathbf{C}_{N_x}^1] & [\mathbf{B}_1^1] & \dots & [\mathbf{B}_1^{N_x}] & [\mathbf{K}_1^1] & .. & [\mathbf{K}_1^{N_y}] & [\mathbf{L}_1^1] & \dots & [\mathbf{L}_1^{N_y}] \\
\vdots & \vdots & \vdots & \vdots & \vdots & \vdots & \vdots & \vdots & \vdots & \vdots & \vdots & \vdots \\
[\mathbf{C}_1^{N_x}] & \dots & [\mathbf{C}_{N_x}^{N_x}] & [\mathbf{B}_{N_x}^1] & \dots & [\mathbf{B}_{N_x}^{N_x}] & [\mathbf{K}_{N_x}^1] & \dots & [\mathbf{K}_{N_x}^{N_y}] & [\mathbf{L}_{N_x}^1] & \dots & [\mathbf{L}_{N_x}^{N_y}] \\
\hline
[\mathbf{E}_1'^1] & \dots & [\mathbf{E}_{N_x}'^1] & [\mathbf{F}_1'^1] & \dots & [\mathbf{F}_{N_x}'^1] & [\mathbf{A}_1'^1] & \dots & [\mathbf{A}_{N_x}'^1] & [\mathbf{C}_1'^1] & \dots & [\mathbf{C}_{N_x}'^1] \\
\vdots & \vdots & \vdots & \vdots & \vdots & \vdots & \vdots & \vdots & \vdots & \vdots & \vdots & \vdots \\
[\mathbf{E}_1'^{Ny}] & \dots & [\mathbf{E}_{N_x}'^{Ny}] & [\mathbf{F}_1'^{Ny}] & \dots & [\mathbf{F}_{N_x}'^{Ny}] & [\mathbf{A}_1'^{Ny}] & \dots & [\mathbf{A}_{N_x}'^{Ny}] & [\mathbf{C}_1'^{Ny}] & \dots & [\mathbf{C}_{N_x}'^{Ny}] \\
\hline
[\mathbf{K}_1'^1] & \dots & [\mathbf{K}_{N_x}'^1] & [\mathbf{F}_1'^1] & \dots & [\mathbf{F}_{N_x}'^1] & [\mathbf{C}_1'^1] & \dots & [\mathbf{C}_{N_x}'^1] & [\mathbf{B}_1'^1] & \dots & [\mathbf{B}_{N_x}'^1] \\
\vdots & \vdots & \vdots & \vdots & \vdots & \vdots & \vdots & \vdots & \vdots & \vdots & \vdots & \vdots \\
[\mathbf{K}_1^{Ny}] & \dots & [\mathbf{K}_{N_x}'^{Ny}] & [\mathbf{L}_1'^{Ny}] & \dots & [\mathbf{L}_{N_x}'^{Ny}] & [\mathbf{C}_1'^{Ny}] & \dots & [\mathbf{C}_{N_x}'^{Ny}] & [\mathbf{B}_1'^{Ny}] & \dots & [\mathbf{B}_{N_x}'^{Ny}]
\end{array}\right], \tag{A.1}$$

where

$$a_i^j(q,n)=\begin{cases}\sum_p\sum_m A_{mnpq}\varphi_m(x_j)\varphi_p(x_i)+\dfrac{1}{Z_n^i} \;\; for \;\; i=j=1,\dots,N_x; \quad q=n=1,\dots,n\_\max,\\ \sum_p\sum_m A_{mnpq}\varphi_m(x_j)\varphi_p(x_i) \;\; for \;\; i=j=1,2,\dots,N_x; \quad q\neq n=1,2,\dots,n\_\max,\\ \sum_p\sum_m A_{mnpq}\varphi_m(x_j)\varphi_p(x_i) \;\; for \;\; i\neq j=1,2,\dots,N_x,\end{cases} \tag{A.2}$$

where $a_i^j(q,n)$ is the component of matrix $[\mathbf{A}_i^j]$ at row q and column n. In the same way, the components of the other matrixes can be written as follows:

$$c_i^j(q,n)=\sum_p\sum_m A_{mnpq}\varphi'_m(x_j)\varphi_p(x_i) \quad for \;\; i,j=1,\dots,N_x; \quad q,\; n=1,\dots,n\_\max, \tag{A.3}$$

$$e_i^j(q,m)=\sum_p\sum_n A_{mnpq}\varphi_n(y_j)\varphi_p(x_i) \quad for \;\; i=1,\dots,N_x,\; j=1,\dots,N_y; \quad m=1,\dots,m\_\max; \quad q=1,\dots,n\_\max, \tag{A.4}$$

$$f_i^j(q,m)=\sum_p\sum_n A_{mnpq}\varphi'_n(y_j)\varphi_p(x_i) \quad for \;\; i=1,\dots,N_x,\; j=1,\dots,N_y; \quad m=1,\dots,m\_\max; \quad q=1,\dots,n\_\max, \tag{A.5}$$

$$b_i^j(q,n)=\begin{cases}\sum_p\sum_m A_{mnpq}\varphi_m(x_j)\varphi'_p(x_i)+\dfrac{1}{Z_{Tn}^i} \;\; for \;\; i=j=1,2,\dots,N_x; \quad q=\; n=1,2,\dots,n\_\max,\\ \sum_p\sum_m A_{mnpq}\varphi_m(x_j)\varphi''_p(x_i) for \;\; i=j=1,2,\dots,N_x; \quad q\neq\; n=1,2,\dots,n\_\max,\\ \sum_p\sum_m A_{mnpq}\varphi_m(x_j)\varphi'_p(x_i) \;\; for \;\; i\neq j=1,2,\dots,N_x,\end{cases} \tag{A.6}$$

$$k_i^j(q,m)=\sum_p\sum_n A_{mnpq}\varphi_n(y_j)\varphi'_p(x_i) \;\; for \;\; i=1,\dots,N_x,\; j=1,\dots,N_y; \quad m=1,\dots,m\_\max; \quad q=1,\dots,n\_\max, \tag{A.6'}$$

$$l_i^j(q,m)=\sum_p\sum_n A_{mnpq}\varphi'_m(y_j)\varphi'_p(x_i) \;\; for \;\; i=1,\dots,N_x,\; j=1,\dots,N_y; \quad m=1,\dots,m\_\max; \quad q=1,\dots,n\_\max, \tag{A.7}$$

$$e'_{ij}(p,n)=\sum_q\sum_m A_{mnpq}\varphi_q(y_j)\varphi_m(x_i) \;\; for \;\; i=1,\dots,N_x,\; j=1,\dots,N_y; \quad p=1,\dots,m\_\max; \quad n=1,\dots,n\_\max, \tag{A.8}$$

$$f'_ij(p,n)=\sum_q\sum_m A_{mnpq}\varphi_q(y_j)\varphi'_m(x_i) \;\; for \;\; i=1,\dots,N_x,\; j=1,\dots,N_y; \quad p=1,\dots,m\_\max; \quad n=1,\dots,n\_\max, \tag{A.9}$$

$$a'_i j(p,m)=\begin{cases}\sum_q\sum_n A_{mnpq}\varphi_n(y_j)\varphi_q(y_i)+\dfrac{1}{Z^i_m} \ \text{for}\ i=j=1,\ldots,N_y; \quad p=m=1,\ldots,m\_\max,\\ \sum_q\sum_n A_{mnpq}\varphi_n(y_j)\varphi_q(y_i) \ \text{for}\ i=j=1,\ldots,N_y; \quad p\neq m=1,\ldots,m\_\max,\\ \sum_q\sum_n A_{mnpq}\varphi_n(y_j)\varphi_q(y_i) \ \text{for}\ i\neq j=1,\ldots,N_y,\end{cases} \tag{A.10}$$

$$c'_i j(p,m)=\sum_q\sum_n A_{mnpq}\varphi'_n(y_j)\varphi_q(y_i) \ \text{for}\ i,j=1,\ldots,N_x; \quad p=n=1,\ldots,n\_\max, \tag{A.11}$$

$$k'_i j(p,n)=\sum_q\sum_m A_{mnpq}\varphi_m(x_i)\varphi'_q(y_j) \ \text{for}\ i=1,\ldots,N_x,\ j=1,\ldots,N_y; \quad p=1,\ldots,m\_\max; \quad n=1,\ldots,n\_\max, \tag{A.12}$$

$$l'_i j(p,n)=\sum_q\sum_n Z^{inv}_{mnpq}\varphi'_m(x_i)\varphi'_q(y_j) \ \text{for}\ i=1,\ldots,N_x,\ j=1,\ldots,N_y; \quad p=1,\ldots,m\_\max; \quad n=1,\ldots,n\_\max, \tag{A.13}$$

$$b'^j_i(p,m)=\begin{cases}\sum_q\sum_m A_{mnpq}\varphi_q(y_j)\varphi'_m(x_i)+\dfrac{1}{Z^i_{Tm}} \ \text{for}\ i=j=1,\ldots,N_y; \quad p=\ m=1,\ldots,m\_\max,\\ \sum_q\sum_m A_{mnpq}\varphi_q(y_j)\varphi'_m(x_i) \ \text{for}\ i=j=1,\ldots,N_y; \quad p\neq m=1,\ldots,m\_\max,\\ \sum_q\sum_m A_{mnpq}\varphi_q(y_j)\varphi'_m(x_i) \ \text{for}\ i\neq j=1,\ldots,N_y.\end{cases} \tag{A.14}$$

Matrix $[\psi]$ in Eq. (22) is rectangular with dimensions $(2N_x\, n\_\max+2N_y\, m\_\max)(n\_\max\times m\_\max)$:

$$[\psi]=\begin{bmatrix}\varphi^1_{x_1}0 & \ldots & \varphi^{N_x}_{x_1}0 & \ldots & \varphi'^{N_x}_{x_1}0 & \ldots & \varphi'^1_{x_1}0 & \ldots & \varphi^1_{y_1}0 & \ldots & \varphi^{N_x}_{y_1}0 & \ldots & \varphi'^1_{y_1}0 & \ldots & \varphi'^{N_y}_{y_1} & \ldots & 0\\ 0 & \varphi^1_{x_1}0 & \ldots & \varphi^{N_x}_{x_1}0 & \ldots & \varphi'^{N_x}_{x_1}0 & \ldots & \varphi'^1_{x_1}0 & & \varphi^1_{y_2}0 & & \ldots & & \varphi'^1_{y_2}0 & \ldots & \varphi'^{N_y}_{y_2} & \ldots & 0\\ \vdots & & \vdots & & \vdots & & & \vdots & & \vdots & & & & & \vdots & \vdots & & \\ 0\ldots & & \varphi^1_{x_1}0 & \ldots & \varphi^{N_x}_{x_1}0 & \ldots & \varphi'^{N_x}_{x_1}0 & \ldots & \varphi'^1_{x_1}0 & \ldots & \varphi^1_{y_{n\_\max}}0 & \ldots & \varphi^{N_x}_{y_{n\_\max}}0 & \ldots & \varphi'^1_{y_{n\_\max}}0 & \ldots & \varphi'^{N_y}_{y_{n\_\max}} & 0\\ \vdots & \vdots & & & & & \vdots & \vdots & & & & & \vdots & & \vdots & & \vdots & \\ \vdots & \vdots & & \vdots & & & \vdots & & \vdots & & \vdots & & \vdots & & \vdots & & \vdots & \\ 0\ldots & & \varphi^1_{x_{m\_\max}}0 & \ldots & \varphi^{N_x}_{x_{m\_\max}}0 & \ldots & \varphi'^{N_x}_{x_{m\_\max}}0 & \ldots & \varphi'^1_{x_{m\_\max}}0 & \ldots & \varphi^1_{y_{n\_\max}}0 & \ldots & \varphi^1_{y_1}0 & \ldots & \varphi'^{N_x}_{y_{n\_\max}}0 & \ldots & \varphi'^{N_y}_{y_{n\_\max}} & 0\end{bmatrix}. \tag{A.15}$$

where

$$\varphi^i_{xm}=\sin\left(\frac{m\pi x_i}{L_x}\right) \quad \text{for}\ i=1,\ldots,N_x,\ m=1,\ldots,m\_\max,$$
$$\varphi'^i_{xm}=\cos\left(\frac{m\pi x_i}{L_x}\right)\frac{m\pi}{L_x} \ \text{for}\ i=1,\ldots,N_x,\ m=1,\ldots,m\_\max, \tag{A.16}$$

$$\varphi^i_{yn}=\sin\left(\frac{n\pi y_i}{L_y}\right) \ \text{for}\ j=1,\ldots,N_y,\ n=1,\ldots,n\_\max,$$
$$\varphi'^j_{yn}=\cos\left(\frac{n\pi y_i}{L_x}\right)\frac{n\pi}{L_x} \ \text{for}\ j=1,\ldots,N_y,\ n=1,\ldots,n\_\max. \tag{A.17}$$

Vector $\{\mathbf{H}\}$ in Eq. (22) with dimension $(2N_x\, n\_\max+2N_y\, m\_\max)$ is given by

$$\{H\}=[s^1_1,\ldots,s^1_{n\_\max},\ldots,s^{N_x}_1,\ldots,s^{N_x}_{n\_\max},\ s'^1_1,\ldots,s'^1_{n\_\max},\ldots,s'^{N_x}_1,\ldots,s'^{N_x}_{n\_\max},t^1_1,$$
$$\ldots,t^1_{n\_\max},\ldots,t^{N_x}_1,\ldots,t^{N_x}_{n\_\max},t'^1_1,\ldots,t'^1_{n\_\max},\ldots,t'^{N_x}_1,\ldots,t'^{N_x}_{n\_\max}], \tag{A.18}$$

where

$$s^i_q=\sum_p\sum_m\sum_n A_{mnpq}P_{mn}\varphi_p(x_i) \ \text{for}\ q=1,\ldots,n\_\max,\ i=1,\ldots,N_x,$$
$$t^j_p=\sum_q\sum_m\sum_n A_{mnpq}P_{mn}\varphi_q(y_i) \ \text{for}\ p=1,\ldots,m\_\max,\ j=1,\ldots,N_y,$$
$$s'^i_q=\sum_p\sum_m\sum_n A_{mnpq}P_{mn}\varphi'_p(x_i) \ \text{for}\ q=1,\ldots,n,\ i=1,\ldots,N_x,$$
$$t'^j_p=\sum_q\sum_m\sum_n A_{mnpq}P_{mn}\varphi'_q(y_i) \ \text{for}\ p=1,\ldots,m\_\max,\ j=1,\ldots,N_y. \tag{A.19}$$

Using (A.1), (A.13) and (A.16), Eq. (22) can be written as

$$\{W\}=[A][\{P\}-[M]\{\mathbf{H}\}^T_1-[M]\{\mathbf{H}\}^T_2] \tag{A.20}$$

where $[M]$ is $(2N_x\, n\_\max + 2N_y\, m\_\max)(n\_\max \times m\_\max)$ matrix and the vectors $\{\mathbf{H}\}_1$, $\{\mathbf{H}\}_2$ are given by

$$\{H\}_1 = \left[s_1^1, \ldots, s_{n\_\max}^1, \ldots, s_1^{N_x}, \ldots, s_{n\_\max}^{N_x}, s_1^1, \ldots, s'^1_{n\_\max}, \ldots, s'^{N_x}_1, \ldots, s'^{N_x}_{n\_\max}, 0 \ldots 0\right], \tag{A.21}$$

$$\{H\}_2 = [0 \ldots 0, t_1^1, \ldots, t_{n\_\max}^1, \ldots, t_1^{N_x}, \ldots, t_{n\_\max}^{N_x}, t'^1_1, \ldots, t'^1_{n\_\max}, \ldots, t'^{N_x}_1, \ldots, t'^{N_x}_{n\_\max}]. \tag{A.22}$$

By multiplying, we easily obtain the expression of modal displacement

$$W_{mn} = \sum_p \sum_q A_{mnpq} \left[P_{pq} - \sum_k^{m\_\max} \sum_l^{n\_\max} \sum_g^{m\_\max} \sum_h^{n\_\max} \sum_j^{N_x} P_{kl} \alpha^{0i}_{k\,lg\,h} - \sum_{k'}^{m\_\max} \sum_{l'}^{n\_\max} \sum_{g'}^{m\_\max} \sum_{h'}^{n\_\max} \sum_j^{N_y} P_{k'l'} \beta^{0j}_{k'l'g'h'} \right]. \tag{A.23}$$

This expression can be simplified as

$$W_{mn} = \sum_p \sum_q A_{mnpq} \left[P_{pq} - \sum_k^{m\_\max} \sum_l^{n\_\max} \sum_i^{N_x} P_{kl} \alpha^i_{kl} - \sum_{k'}^{m\_\max} \sum_{l'}^{n\_\max} \sum_j^{N_y} P_{k'l'} \beta^j_{k'l'} \right]. \tag{A.24}$$

References

[1] A.W. Leissa, Vibration of plates, NASA SP-160, 1969.
[2] W. Soedel, *Vibrations of Shells and Plates*, Marcel Dekker, 2004.
[3] K.T. Sundara Raja Iyengar, R. Narayana Iyengar, Determination of the orthotropic plate parameters of stiffened plates and grillages in free vibration, *Applied Scientific Research* 17 (6) (1967) 422–438.
[4] M. Heckl, Wave propagation on beam-plate systems, *Journal of the Acoustical Society of America* 33 (1961) 640–651.
[5] D.J. Mead, A general theory of harmonic wave propagation in linear periodic system with multiple coupling, *Journal of Sound and Vibration* 27 (1973) 235–260.
[6] D.J. Mead, Wave propagation and natural modes in periodic systems: II. Multi-coupled systems, with and without damping, *Journal of Sound and Vibration* 40 (1975) 19–39.
[7] Y. Yong, Y.K. Lin, Propagation of decaying waves in periodic and piecewise periodic structures of finite length, *Journal of Sound and Vibration* 129 (1989) 99–118.
[8] A.K. Roy, R. Plunkett, Wave attenuation in periodic structures, *Journal of Sound and Vibration* 104 (1986) 395–410.
[9] B.A.J. Mustafa, R. Ali, Prediction of natural frequency of vibration of stiffened cylindrical shells and orthogonally stiffened curved panels, *Journal of Sound and Vibration* 113 (1987) 317.
[10] M. Barrette, A. Berry, O. Beslin, Vibration of stiffened plates using hierarchical trigonometric functions, *Journal of Sound and Vibration* 235 (8) (2000) 727–747.
[11] D.W. Fox, V.G. Sigillito, Bounds for frequencies of rib reinforced plates, *Journal Sound and Structural Vibration* 69 (4) (1982) 497–507.
[12] D.W. Fox, V.G. Sigillito, Bounds for eigen frequencies of a plate with an elastically attached reinforcing rib, *International Journal of Solids and Structures* 18 (3) (1982) 235–247.
[13] E.J. Sapountzakis, J.T. Katsikadelis, Dynamic analysis of elastic plates reinforced with beams of doubly-symmetrical cross section, *Computational Mechanics* 23 (1999) 429–430.
[14] U. Orrenius, S. Finnveden, Calculation of wave propagation in rib stiffened plate structures, *Journal of Sound and Vibration* 198 (1996) 203–224.
[15] J.-H. Lee, J. Kim, Analysis of sound transmission through periodically stiffened panels by space harmonic expansion, *Journal of Sound and Vibration* 251 (2) (2002) 349–366.
[16] D.J. Mead, K.K. Pujara, Space-harmonic analysis of periodically supported beams: response to convected random loading, *Journal of Sound and Vibration* 14 (1971) 525–541.
[17] D.J. Mead, Free wave propagation in periodically supported, infinite beams, *Journal of Sound and Vibration* 11 (1970) 181–197.
[18] D.J. Mead, Wave propagation in continuous periodic structures: research contributions from Southampton, *Journal of Sound and Vibration* 190 (1996) 495–524.
[19] C. Maurys, P.O. Matte, Sound transmission through a rib-stiffened plate comparison of light-fluid approximation with experimental results, *Journal of Sound and Vibration* 249 (1) (2002) 206–212.
[20] T.R. Lin, J. Pan, A closed form solution for the dynamic response of finite ribbed plates, *Journal of the Acoustical Society of America* 119 (2) (2006) 917–925.
[21] T.R. Lin, A study of modal characteristics and the control mechanism of finite periodic and irregular ribbed plates, *Journal of the Acoustical Society of America* 123 (2) (2008) 729–737.
[22] P.G. Bremner, Vibro-acoustics of ribbed structures—a compact modal formulation for SEA models. *Proceedings of the Noise-Con 94*, Ft. Lauderdale, Florida, May 1994.
[23] V. Cotoni, R.S. Langley, P.J. Shorter, A statistical energy analysis subsystem formulation using finite element and periodic structure theory, *Journal of Sound and Vibration* 318 (2008) 1077–1108.
[24] G. Maidanik, Response of ribbed panels to reverberant acoustic fields, *Journal of the Acoustical Society of America* 34 (6) (1962) 809–826.
[25] F. Fahy, *Sound and Structural Vibration: Radiation, Transmission and Response*, Academic Press, London, 1985.
[26] W.R. Graham, A comparison of models for the wavenumber–frequency spectrum of turbulent boundary layer pressures, *Journal of Sound and Vibration* 206 (1997) 541–565.
[27] F. Han, R.J. Bernhard, L.G. Mongeau, A model for the vibro-acoustic response of plates excited by complex flows, *Journal of Sound and Vibration* 246 (5) (2001) 901–926.
[28] E.E. Ungar, Transmission of plate flexural waves through reinforcing beams dynamic stress concentrations, *Journal of the Acoustical Society of America* 33 (5) (1961) 633–639.
[29] B.R. Mace, The response of a fluid-loaded, beam-stiffened plate, *Journal of Sound and Vibration* 79 (3) (1981) 439–542.
[30] F.G. Leppington, E.G. Broadbente, K.H. Heron, The acoustic radiation efficiency from rectangular panels, *Proceedings of the Royal Society of London, A* 382 (1982) 245–271.
[31] J.A. Cockburn, J.E. Robertson, Vibration response of spacecraft shrouds to in-flight fluctuating pressures, *Journal of Sound and Vibration* 33 (4) (1974) 399–425.
[32] G.M. Corcos, Resolution of pressure in turbulence, *Journal of the Acoustical Society of America* 53 (2) (1963) 192–199.
[33] B.M. Efimtsov, Characteristics of the field of turbulent wall pressure fluctuations at large Reynolds numbers, *Soviet Physics—Acoustics* 28 (4) (1982) 289–292.
[34] ESI Group, *VAone 2006 User's Guide*, 2006.

[35] MSC.Software Corporation, Santa Ana, CA. *MSC Nastran 2007 rl: release Guide*, 2007.
[36] B. Lui, L. Feng, A. Nilsson, Sound transmission through curved aircraft panels with stringer and ring attachments, *Journal of Sound and Vibration* 300 (2007) 949–973.
[37] J.L. Guyder, B. laulagnet, Structural acoustic radiation prediction: expanding the vibratory response on a functional basis, *Applied Acousctics* 33 (4) (1974) 399–425.
[38] E.P. Popov, *Mechanics of Materials*, Prentice Hall, 1976.
[39] B.L. Clarkson, R.J. Pope, Experimental determination of modal density and loss factor for plat panel and cylinders, *Journal of Sound and Vibration* 77 (4) (1981) 535–549.
[40] B. Lui, Noise radiation of aircraft panels subjected to boundary layer pressure fluctuations, *Journal of Sound and Vibration* 314 (2008) 693–711.
[41] M.M. Makulas, J.A. McElman, On the free vibrations of eccentrically stiffened cylindrical shells and flat plate, *NASA* TN D-3010.
[42] V. Smol'Yakov, V.M. Tkachenko, Model of a field of pseudosonic turbulent wall pressures and experimental data, *Soviet Physics, Acoustics* 37 (6) (1991) 627–631.
[43] D.M. Chase, The character of the turbulent wall pressure spectrum at subconvective wavenumbers and a suggested comprehensive model, *Journal of Sound and Vibration* 112 (2) (1987) 125–147.
[44] C. Lesueur, 1988, Rayonnement acoustique des structures *Vibroacoustique, Interactions Fluid–Structure* (Acoustic radiation of the structures, *Vibroacoustic, Fluid–Structures Interaction*), Eyrolles.